HHS Public Access

Author manuscript

Nat Struct Mol Biol. Author manuscript; available in PMC 2016 March 01.

Published in final edited form as:

Nat Struct Mol Biol. 2015 September ; 22(9): 736–743. doi:10.1038/nsmb.3072.

Recruitment and activation of the ATM kinase in the absence of DNA damage sensors

Andrea J. Hartlerode[1], **Mary J. Morgan**[1], **Yipin Wu**[1], **Jeffrey Buis**[1], and **David O. Ferguson**[1,2]

[1]Department of Pathology, The University of Michigan Medical School, Ann Arbor, MI 48109. USA

Abstract

Two kinases, ATM and DNA-PKcs, control rapid responses to DNA double-strand breaks (DSBs). The paradigm for ATM control is recruitment and activation by the Mre11–Rad50–NBS1 (MRN) sensor complex, whereas DNA-PKcs requires the sensor Ku (Ku70–Ku80). Using *Mus musculus* cells harboring targeted mutant alleles of *Mre11* and/or *Ku70*, together with pharmacologic kinase inhibition we demonstrate that ATM can in fact be activated by DSBs in the absence of MRN. When MRN is deficient, DNA-PKcs efficiently substitutes for ATM in facilitating local chromatin responses. Strikingly, in the absence of both MRN and Ku, ATM is recruited to chromatin, phosphorylates H2AX, and triggers the G2/M cell cycle checkpoint, but DNA repair functions of MRN are not restored. This implies that a complex interplay between sensors plays a significant role in ATM control, rather than straightforward recruitment and activation by MRN.

DNA double-strand breaks (DSBs) are a highly toxic form of DNA damage and a potent cause of genome instability. In eukaryotes, two major pathways exist to repair DSBs: homology-directed repair (HDR) and non-homologous end-joining (NHEJ). Prior to actual repair, systems must be in place to detect DNA lesions and initiate signaling cascades that alter many aspects of cellular physiology. Collectively these DNA damage responses are comprised of an intricate network of proteins in a complex choreography of events. Failure to correctly repair DSBs can lead to carcinogenesis as well as neurological and developmental disorders[1]. In addition, radiotherapy and many anti-cancer therapeutics are based on killing of tumor cells by DSB induction.

---

[2]Corresponding author: David O. Ferguson, The University of Michigan Medical School, 109 Zina Pitcher Place – room 2067, Ann Arbor, MI 48109–2200, tel (734) 764–4591, fax (734) 763–2162, daviferg@umich.edu.

Author Contributions: AJH planned and performed most experiments, analyzed/interpreted the resulting data, and participated in writing all portions of the manuscript. YW performed and interpreted experiments in Fig. 7d and e, and Supplementary Fig. 6 and 7e. MJM performed and interpreted immunoflourescent foci experiments in Fig. 5c and Supplementary Fig. 3c, 3d, and 4, and assisted AJH with the laser microirradiation experiments in Fig. 2a and 6. JB performed initial mouse breedings and analyses of Mendelian inheritance (Supplementary Table 1). DOF participated in the design of all experiments as well as analyses and interpretation of data, and in writing of the manuscript.

The authors declare no competing financial interests.

At the beginning of this dance are two highly conserved multiprotein complexes, MRN (Mre11–RAD50–NBS1) and Ku (Ku70–Ku80), which are considered the primary sensors of DSBs[2,3]. Both complexes are then thought to recruit and activate a unique member of the phosphatidylinositol 3-kinase-related kinase (PIKK) family of serine/threonine kinases, ATM and DNA-PKcs respectively[4,5]. While much has been learned about how MRN and Ku function in isolation to recruit their respective kinases, little is known about how they may influence each other at DSBs during the damage response *in vivo*. Furthermore, it remains unclear why in most metazoans two separate kinases function in the DSB response and how activation of either kinase is accomplished in the context of seemingly redundant sensors.

The ATM kinase functions at the apex of the DSB signaling cascade to coordinate many cellular outcomes, and in order to carry out these functions has a vast network of target substrates[6]. Inherited *ATM* mutations cause ataxia telangiectasia (AT), a syndrome with diverse sequelae including cancer predisposition, neuro-degeneration, and immune dysfunction[7]. Our current understanding of ATM activation is that the MRN complex functions as the DSB sensor, directly binding DSBs to recruit and activate ATM[5,8-12] (Fig. 1a). A role for MRN in the activation of ATM is supported by the AT-like features of human syndromes resulting from MRN mutations, as well as defective ATM activation in MRN mutant cells, and the enhancement of ATM kinase activity by MRN *in vitro*[7,12-15].

The Ku complex also binds DSBs, but specifically activates the DNA-PKcs kinase, and together these proteins make up the DNA-PK holoenzyme[16]. Ku is one of the most abundant cellular proteins, and exhibits high affinity for double-stranded DNA ends[17]. Unlike the many functions of ATM, the primary role of DNA-PK is direct participation in DSB repair via NHEJ. In this role DNA-PKcs itself is the most well characterized substrate of the DNA-PK holoenzyme[18]. Mice lacking DNA-PKcs, and those lacking Ku70 or Ku80, are immunodeficient due to defective V(D)J recombination, which requires NHEJ[19,20].

It is clear that the cellular response to DSBs is a sophisticated web of operations involving many proteins that must be tightly regulated in order to generate the necessary outcome. A deeper understanding of these processes is key to decoding the pathogenesis of cancer and designing successful treatments for this disease. However, unraveling this web is a difficult challenge. To gain mechanistic understanding of the earliest events in the mammalian DSB response we examined cells lacking one or both of the DSB sensor complexes. We discovered that removal of Ku in the absence of the MRN complex restores several ATM-dependent responses, demonstrating that MRN is not absolutely required for recruitment and activation of ATM.

Results

Generation of MRN- and MRN/Ku-deficient cells

We disabled the MRN complex through use of mouse embryonic fibroblasts (MEFs) that originally harbored one Mre11 null allele (*Mre11*$^{-}$), and one Cre/LoxP conditional allele (*Mre11*^{cond}) (Fig. 1b). Exposure to Cre recombinase via adenovirus converted these cells to *Mre11*$^{-/-}$, which also causes deficiency of Rad50 and NBS1 (termed MRN deficiency),

presumably due to instability of the proteins in the absence of Mre11[14] (Fig. 1c and Supplementary Fig. 1). Control cells used for experiments were initially *Mre11*$^{cond/+}$, which were converted to *Mre11*$^{-/+}$ via Cre recombinase in parallel with other genotypes to control for effects of viral delivery of Cre and for LoxP recombination at a target locus. Through mouse breeding, we also generated MEFs of these MRN genotypes combined with germline knockout of Ku70 (*Ku70*$^{-/-}$). Removal of Ku70 does not require use of a conditional allele, and causes deficiency of its heterodimeric partner Ku80 (termed Ku deficiency)[21] (Fig. 1c and Supplementary Fig. 1).

Rapid recruitment of MRN and Ku to DNA damage

To gain understanding of the interplay between sensor complexes in the immediate aftermath of DSB induction we used live cell imaging to examine localization of MRN and Ku to DNA damage. GFP-tagged NBS1 was used to track MRN recruitment to laser-induced damage in real time. MRN is recruited by 15 to 30 seconds after damage and Ku deficiency did not appear to impact its recruitment (Fig. 2a). Ku was tracked by introducing both GFP-tagged Ku70 and Ku80, and its recruitment proved to be faster than laser stripes could be generated. Instead, we pulsed the laser at a single location while simultaneously recording video instead of time-lapse images. Within one second post-damage, Ku could be detected at sites of damage and it continued to accumulate for approximately 10 seconds in most cells (Fig. 2b, Supplementary Fig. 2 and Supplementary Movie 1). Loss of the MRN complex did not appear to impact Ku recruitment. Therefore, immediately following DNA damage, the absence of either sensor does not substantially impact overall accumulation of the other.

Restoration of the G2/M checkpoint in MRN/Ku-deficient cells

The ATM kinase controls a crucial DNA damage checkpoint at the transition between the G2 and M phases of the cell cycle[11]. This checkpoint prevents the passage of broken chromosomes to daughter cells, and its absence contributes to the cancer predisposition observed in patients with AT or certain inherited mutations in MRN genes[13]. We analyzed the G2/M checkpoint by assessing the impact of ionizing radiation (IR) on the mitotic index, as measured by the percentage of cells positive for the mitosis entry marker phospho-histone H3 serine 10. An intact checkpoint is reflected by a substantial reduction in the percentage of mitotic cells after IR (reduced mitotic index), whereas a defective checkpoint manifests as a comparatively higher percentage of cells passing into M phase (higher mitotic index).

As anticipated, we observed higher percentages of *ATM*$^{-/-}$ and *Mre11*$^{-/-}$ cells in M phase after IR[22,23] (Fig. 3a). Unexpectedly, cells lacking both Mre11 and Ku70 displayed an intact G2/M checkpoint. Given the absence of both sensors, this suggested that another kinase (other than DNA-PKcs) may be substituting for ATM, or that the G2/M checkpoint does not require a kinase. Strikingly, when we performed these experiments in the presence of pharmacologic inhibitors of ATM or DNA-PKcs, the G2/M checkpoint proved to be dependent on ATM (Fig. 3b). Thus, the requirement for MRN in the ATM-dependent G2/M checkpoint appears to be alleviated by the absence of Ku.

MRN DNA repair functions are not rescued by Ku deficiency

In addition to initiating signaling, MRN and Ku function directly in the repair of DSBs. The bypass of MRN's requirement in activating the ATM-dependent G2/M checkpoint raises the possibility that requirements for MRN during DSB repair may be alleviated through removal of Ku. This notion is supported by studies in budding or fission yeast demonstrating that the IR-induced lethality of Mre11 deficiency is suppressed by deletion of Ku[24,25]. We therefore examined the impact of Ku deficiency on MRN-dependent repair functions by examining IR sensitivities and the efficiencies of HDR in cells lacking one or both sensors. Based on the IR sensitivity of *Mre11*$^{-/-}$*Ku70*$^{-/-}$ cells we find no evidence for rescue of IR hypersensitivity by removal of Ku (Fig. 4a). We used an integrated DR-GFP reporter assay to measure HDR[26] (Fig. 4b). The *Mre11*$^{c/-}$ genotype indicates the parental cell line with two distinct *Mre11* alleles (conditional (c) and null (–)). To provide matched controls for Mre11 deletion, cells were either treated with Adeno-Cre recombinase to generate *Mre11*$^{-/-}$ or an empty adenovirus to maintain the *Mre11*$^{c/-}$ genotype. Mre11 deficiency reduced HDR while Ku deficiency elevated HDR relative to that of control cells (Fig. 4c), as has been reported previously[14,26]. In Ku-deficient cells, further removal of Mre11 reduced HDR by a percentage similar to that caused by Mre11 removal in control cells (Fig. 4d). Therefore we find no evidence for rescue of MRN-dependent HDR by Ku deficiency (Fig. 4c and d). This is consistent with our finding that Ku70 deficiency provides no rescue of *Mre11*$^{-/-}$ early mouse embryonic lethality (Supplementary Table 1), as functional HDR is required to transit early embryonic development[27]. All told, these findings indicate that in mammals removal of Ku can largely bypass the need for MRN to activate the ATM-dependent G2/M checkpoint, but not to facilitate homology-directed DSB repair.

ATM recruitment and activation in the absence of MRN and Ku

ATM is rapidly recruited to chromatin in the vicinity of DSBs[28]. This recruitment has been presumed to require interaction with MRN. We therefore assessed whether ATM is recruited to chromatin in the absence of MRN and Ku using cellular fractionation. We observed IR-induced chromatin localization of ATM in control cells (*Mre11*$^{+/-}$*Ku70*$^{+/+}$) but not in MRN-deficient cells (*Mre11*$^{-/-}$*Ku70*$^{+/+}$) (Fig. 5a and Supplementary Data Set 1). Strikingly, when Ku is also absent (*Mre11*$^{-/-}$*Ku70*$^{-/-}$) ATM chromatin localization is restored. Thus, the absence of Ku reveals that MRN is not strictly required for DNA damage-induced ATM chromatin localization.

To further understand ATM recruitment and the intact ATM-dependent checkpoint in the absence of DSB sensors we examined one of the earliest signaling events in the DSB response, phosphorylation of histone H2AX. This specialized histone is present in 2 to 25% of nucleosomes, depending on cell type, and is phosphorylated (termed γH2AX) for megabase regions on either side of a DSB[29]. γH2AX then serves as a platform for more extensive chromatin changes that are required to propagate DNA damage responses[11] (Fig. 1a). We induced DSBs by exposing MEFs to IR and measured total cellular γH2AX formation by immunoblotting. In addition, we determined the relative contributions of ATM and DNA-PKcs to this signaling by pre-treating cells with specific pharmacologic kinase inhibitors.

In control cells (*Mre11*$^{+/-}$) the ATM inhibitor markedly reduced H2AX phosphorylation whereas DNA-PKcs inhibition had little impact (Fig. 5b and Supplementary Data Set 1). In contrast, the opposite pattern was observed in MRN-deficient cells (*Mre11*$^{-/-}$), wherein the DNA-PKcs inhibitor reduced H2AX phosphorylation to near background levels. This is consistent with models depicting a requirement for MRN in ATM recruitment and activation[9-11] (Fig. 1a), and demonstrates that DNA-PKcs can very efficiently substitute for ATM in phosphorylating H2AX when MRN is absent (Fig. 5b and Supplementary Data Set 1). In *Mre11*$^{-/-}$*Ku70*$^{-/-}$ cells we observed substantial levels of γH2AX after IR. Importantly, this phosphorylation returned to being ATM-dependent (Fig. 5b and Supplementary Data Set 1). To determine if this sensor-independent ATM activity is restricted to H2AX phosphorylation we examined other ATM-dependent DNA damage response events (Supplementary Fig. 3). IR-induced phosphorylation of Kap1 and SMC1 were both observed (Supplementary Fig. 3a). Like H2AX, the degree of phosphorylation appeared less than in control cells (approximately one third of control levels for pKap1), but was fully ATM-dependent (Supplementary Fig. 3b).

Immunoblotting assesses γH2AX levels averaged across the genome in a cell population. γH2AX formation normally occurs in the vicinity of DSBs, and can be visualized by immunofluorescence as punctate nuclear foci[29]. Therefore, to determine if H2AX phosphorylation is distributed normally in the absence of DSB sensors, we compared γH2AX focus formation. In agreement with immunoblot data (Fig. 5b), we observe that γH2AX foci formation shifts dependency from ATM to DNA-PKcs when MRN is absent (Fig. 5c and Supplementary Fig. 4). Importantly, when Ku is also removed dependency returns to ATM. In each genotype the majority of cells (65 to 80%) contained 10 or more γH2AX foci and the morphology of these foci were all similar (Fig. 5c and Supplementary Fig. 4). Thus, as in normal cells, ATM activated in the absence of MRN and Ku is recruited to chromatin in the vicinity of DSBs to phosphorylate H2AX.

Rapid MDC1 recruitment in the absence of MRN and Ku

After H2AX is phosphorylated it is bound by mediator of DNA damage checkpoint 1 (MDC1)[30,31]. MDC1 then promotes recruitment of DNA damage response and checkpoint proteins to the chromatin flanking DSBs, which ultimately leads to initiation of the G2/M cell cycle checkpoint[31-33]. To gain further insight into the newly discovered MRN-independent ATM activation and G2/M checkpoint initiation, we examined GFP-tagged MDC1 recruitment using live cell imaging after laser microirradiation[34]. This approach permits visualization of recruitment within seconds to minutes after damage, far faster than timescales permitted in immunofluorescence-based experiments. Thus, ATM activation can be compared within the earliest timeframe of the DNA damage response.

We observe MDC1 recruitment by 15 seconds, and this is dependent on ATM in control and Ku-deficient cells[30] (Fig. 6). When MRN is rendered deficient, MDC1 accumulates as rapidly and intensely as in control cells. However, this recruitment is now dependent on DNA-PKcs (Fig. 6). Thus even during the rapid events immediately following damage, DNA-PKcs can locally substitute for ATM when MRN is absent. Further removal of Ku (MRN/Ku-deficient) had little impact on MDC1 recruitment causing only a subtle delay of

less than 15 seconds, but strikingly this robust recruitment was ATM-dependent (Fig. 6). Therefore, even within the first minute of the DSB response, ATM can function in the absence of MRN and Ku.

ATM activation over broad experimental conditions

We further investigated MRN-independent ATM activation by comparing various parameters to ATM activation in control cells. The pattern of γH2AX kinase dependency was determined over a variety of IR doses ranging from 0.5 to 75 Gy, and it did not differ at any dose tested (Supplementary Fig. 5a–c). γH2AX levels were also compared over a timecourse post-IR ranging from 15 minutes to 10 hours (Fig. 7a and Supplementary Fig. 5d). H2AX phosphorylation was readily detected by immunoblotting in MRN/Ku deficiency throughout the timecourse. The peak intensity for both genotypes was similar, though it appeared delayed in MRN/Ku-deficient cells: control cells achieved peak signal intensity by 30 minutes post-IR, whereas *Mre11*$^{-/-}$*Ku70*$^{-/-}$ cells did so 2 hours post-IR (Fig. 7a). In addition, this timecourse reveals that there is a persistence of H2AX phosphorylation in MRN/Ku-deficient cells compared to controls. This result is consistent with the presence of unrepaired DSBs and is not unexpected given the HDR defect caused by Mre11 deficiency (Fig. 4c and d) and the NHEJ defect caused by Ku70 deficiency[21].

End-resection and kinase activation

In the presence of MRN, single-stranded DNA (ssDNA) at a break was shown *in vitro* to be a potent activator of ATM[12]. Recent work has demonstrated the importance of Mre11 nuclease-dependent end-resection in the initiation and choice of DNA repair pathways[2,35], however its role in kinase activation is less understood. To investigate roles of Mre11 nuclease activity we generated Ku null MEFs expressing Mre11 with a targeted single amino acid change (*Mre11*^{H129N}) abrogating DNA nuclease activities, while maintaining normal MRN interactions and structure[14,36] (Fig. 1b). We found that Mre11 nuclease deficiency maintained ATM as the primary kinase following IR, with or without Ku70 (Figure 7b and Supplementary Fig. 6). This demonstrates that H2AX can be efficiently phosphorylated by DNA-PKcs when MRN is absent, but not when a nuclease-deficient version of the complex is present. Therefore MRN-dependent resection appears to be dispensable in the rapid signaling response to DSBs.

The ATR kinase, another PIKK family member that functions in DNA damage responses, is recruited and activated by ssDNA[37]. In certain contexts, it has been shown that ATR can phosphorylate and activate ATM[38]. Although Mre11 nuclease activity is dispensable for rapid signaling after damage, it remains possible that other nucleases could generate the ssDNA necessary to activate ATR[24,25]. To investigate a role for ATR in MRN-independent ATM activation we used a specific ATR kinase inhibitor to examine DNA repair signaling in cells lacking MRN and Ku[39]. Phosphorylation of Chk1 at S345 is an established target of the ATR kinase and is used as a readout of ATR activity and inhibition. We found that similar to control cells, ATM activation by IR in MRN/Ku-deficient cells does not depend on ATR (Fig. 7c).

Our results have shown that in the absence of MRN, DNA-PKcs can very efficiently substitute for ATM in phosphorylating H2AX during the DSB response (Fig. 5b, 7d–f and Supplementary Fig. 3a, 7a, and 7e). However, when MRN is present but dysfunctional (nuclease-deficient), DNA-PKcs has no detectable impact on H2AX phosphorylation (Fig. 7b, 7d, and Supplementary Fig. 7c and e). This suggests that the presence of MRN at DSBs somehow prohibits DNA-PKcs from playing a major role in H2AX phosphorylation. To assess this in more detail we examined H2AX phosphorylation in the presence of the MRN complex, but the absence of the ATM kinase, where another kinase would be needed to phosphorylate H2AX in response to damage. We found that DNA-PKcs has a limited ability to phosphorylate H2AX in the absence of ATM, but not to the levels observed in MRN-deficient cells (Fig. 7d and e and Supplementary Fig. 7d and e). This data supports the hypothesis that the presence of the MRN complex at DSBs hinders the ability of DNA-PKcs to phosphorylate H2AX.

In normal cells that have suffered DSBs, active ATM is auto-phosphorylated at serine 1981 (S1987 in mouse)[40]. While it is established that this auto-phosphorylation site is not required for ATM kinase activity[41], it nonetheless has served as a convenient experimental marker for ATM activation. Curiously, we observe that ATM lacks S1981 phosphorylation in MRN/Ku-deficient cells (Fig. 7f and Supplementary Fig. 5e, 7a and 7b). Therefore, the phosphorylation of ATM S1981 provides a molecular distinction between ATM activated in the presence versus the absence of MRN and Ku.

Discussion

Here we have shown that in the absence of MRN, removal of Ku restores ATM chromatin localization, kinase activation, and the G2/M cell cycle checkpoint. In contrast, DNA repair functions of MRN are not restored in the absence of Ku. These findings reveal that MRN is not absolutely required for recruitment and allosteric activation of ATM, but instead functions to maximize or sustain ATM-dependent DSB responses. Rather than simple recruitment, activation of ATM appears to be strongly influenced by a rapid interplay between MRN and Ku occurring within seconds after DNA damage.

Previous studies have shown that Ku and MRN can compete for binding to DSBs *in vitro*[42], and Ku must be removed from DNA ends to allow for HDR[43,44], together suggesting some amount of competition between MRN and Ku *in vivo*. However, findings from our live cell imaging studies imply that simple competition does not predominate within the earliest seconds of the DSB response (Fig. 2, Supplementary Fig. 2, and Supplementary Movie 1). These studies support the notion that both sensors bind DSBs rapidly, but with Ku binding first and MRN joining shortly thereafter. Neither complex appears to require the other for recruitment to DSBs, and importantly, within this narrow time frame that includes kinase activation, the absence of one sensor does not measurably impact the recruitment of the other. These findings significantly constrain the mechanism at work in the early DSB response. In this context we speculate a level of opposition in the functions of MRN and Ku at DNA ends that does not involve simple competition for initial binding.

In principle, the restoration of ATM function in MRN/Ku deficiency could result from the absence of DNA-PKcs kinase activity, rather than loss of Ku itself. If this were the case, the DNA-PKcs kinase inhibitor would be expected to cause MRN-independent ATM activity and otherwise phenocopy MRN/Ku-deficient cells without the need for Ku deficiency. However, this was not observed in our examinations of ATM substrate phosphorylations and γH2AX kinetics (Fig. 5b, 7c–f and Supplementary Fig. 3a, 5b–c, 7a and 7e). Similarly, our observation that DNA-PKcs can substitute for ATM in phosphorylating H2AX when MRN is absent (Fig. 5b) raises the possibility that increased DNA-PKcs function could result from lack of ATM activity rather than the absence of MRN. As treatment with the ATM inhibitor in control cells did not permit DNA-PKcs to substitute for ATM, this is not likely the case (Fig. 5b, 7c–f and Supplementary Fig. 3a, 5b–c, and 7a). We tested this hypothesis further by examining ATM knockout cells in the presence and absence of the DNA-PKcs inhibitor, followed by comparison γH2AX immunoblot signals (Fig. 7d–e and Supplementary Fig. 7d–e). In the absence of ATM, DNA-PKcs did show a modest ability to phosphorylate H2AX, but levels clearly remained below that observed in MRN-deficient cells, which were indistinguishable from control cells. These findings argue that interplay among the DSB sensors plays the major role in controlling ATM activation, with kinase crosstalk making a more minor contribution.

While not essential for initial ATM activation, we uncovered several lines of evidence which support the notion that MRN maximizes and sustains ATM-dependent responses. Phosphorylation of ATM substrates Kap1 and SMC1 in cells lacking MRN and Ku is not as robust as in control cells (Supplementary Fig. 3a–b and 7a). In both cases IR-induced phosphorylation is fully ATM-dependent, but is reduced by 60 to 70% (Supplementary Fig. 3b). Detailed examination of the timecourse of H2AX phosphorylation revealed that peak levels of γH2AX were similar, but were delayed approximately 1.5 hours in MRN/Ku-deficient cells compared to controls (Fig. 7a). Live cell imaging of γH2AX-dependent MDC1 recruitment demonstrated that MDC1 is rapidly recruited to laser damage in cells of all genotypes examined, but is slightly reduced in MRN/Ku-deficient cells at 15 seconds post-damage (Fig. 6). This level of recruitment is near the limit of detection of the instrument used for this study, thus interpretations must be restrained. Therefore, while antibody based approaches that measure responses over longer times suggest a more substantial delay, live cell imaging indicates that any delay in ATM-dependent signaling in the absence of MRN and Ku is minimal during the critical first minute following DNA damage.

For MRN to influence ATM-dependent DSB responses, it must overcome the more rapid binding by Ku *in vivo*, which is capable of protecting ends[42-44]. The precise nature of how MRN overcomes this protection will require future studies, but the complex could conceivably eject Ku by converting DSBs to ssDNA ends that are a poor substrate for Ku to bind[43,45]. MRN is known to possess two activities that can generate ssDNA: the nuclease activities of Mre11 and ATP-dependent DNA unwinding by Rad50[46]. The endonuclease activity of Mre11 initiates processing at a short distance away from the break and could therefore occur even when Ku is bound[35]. However, we have ruled out a requirement for Mre11 nuclease activity in kinase activation (Fig. 7b, d–e and Supplementary Fig. 6, 7c, and

7e), suggesting a role for Rad50's ATP-dependent DNA unwinding and the recently discovered dramatic conformational changes in Rad50 structure[12,47].

The newly uncovered MRN-independent activation of ATM presented here represents a significant advance in our understanding of the early DSB response. The ability of ATM to function in the absence of MRN helps explain studies of mice engineered to lack the ATM interacting domain of NBS1, which displayed surprisingly minimal AT-like phenotypes[48,49]. The strong requirement for MRN only in the presence of Ku revealed in this study suggests that a key function for MRN in ATM activation is to oppose Ku at DSBs to expose DNA ends. This notion is supported by prior *in vitro* studies[12,15,50], including a study from *Xenopus* oocyte extracts which shows that ATM can be activated in the absence of MRN, but only when relatively higher levels of DNA ends are added[15]. Further studies will be needed to determine if an unknown factor is required for ATM recruitment and activation, or if ATM is in fact activated directly by DNA ends *in vivo*[50].

Online Methods

Growth and analysis of MEFs

All MEFs used in this study were derived in house from day e13.5 embryos and grown in standard culture conditions as described[21]. MEFs tested negative for mycoplasma contamination and genotypes were confirmed by PCR[14] and Western blot (Fig. 1c and Supplementary Fig. 1). Primary MEFs were immortalized by transfection with pBsSVD2005 (SV40 large T antigen expression vector). Adeno-Cre at a MOI of 500 was used. MEFs were grown for 3 days post-infection and split once prior to plating for experiments. Kinase inhibitors were used as follows: ATM, KU55933[51,52] (10μM or 20 μM for 1-2 hrs as indicated, Tocris Biosciences); DNA-PK, NU7026[53,54] (20μM for 2 hrs, Tocris Biosciences); ATR, VE-821[39] (10μM for 2 hrs, Axon Medchem).

Rescue of Embryonic Lethality

Mice are *Mus musculus*, C57B6/129sv mixed background, equal mix of male and female. χ^2 analysis was used to determine the significance of any observed differences between the actual and expected results of the cross performed. No blinding, randomization, or power calculation for sample size was performed. The University of Michigan's University Committee on the Use and Care of Animals (UCUCA) approved all mouse procedures carried out in this study in accordance with an approved protocol.

Western Blots

Cell extracts were prepared in RIPA buffer (150mM NaCl; 1% NP-40; 0.5% $C_{24}H_{39}O_4Na$; 0.1% SDS; 50mM Tris-HCl, pH 8.0) or Laemmli buffer (4% SDS; 20% glycerol; 120 mM Tris-HCl, pH 6.8), resolved by SDS-PAGE and transferred using standard procedures. Primary antibodies were: Mre11 (Cell Signaling, #4895); Rad50 (Bethyl Laboratories, #A300-184A)[55]; NBS1 (Novus Biologicals, #NB110-57272); γH2AX and H2AX (EMD Millipore, #05-636 and #07-627)[56]; pChk1^{S345} (Cell Signaling, #2348); Kap1 (Cell Signaling, #4124); pKap1^{S824} (Bethyl Laboratories, #A300-767A); pSMC1^{S957} (Cell Signaling, #4805); ATM (Cell Signaling, #2873); pATM^{S1981} (Rockland Immunochemicals,

#200-301-400)[55]; Ku70 (Cell Signaling, #4588); Ku86 (Santa Cruz Biotechnology, #sc9034); DNA-PKcs (Kamiya Biomedical, #MC-365); TopoI (BD Biosciences, #556597); and GAPDH (Cell Signaling, #2118). Validation of all primary antibodies unless otherwise referenced was provided by the manufacturer. Secondary antibodies for Western blots were IRDye conjugated goat anti-rabbit or anti-mouse (Li-Cor Biosciences, #925-32210, #925-32211, #925-68070, #925-68071). Original uncropped images of key Western blots in this study can be found in Supplementary Data Set 1.

Quantification of band intensities were determined using Li-Cor Odyssey 2.1 software. For each experiment the level of the appropriate loading control in the unirradiated sample was set to one and any differences in loading amongst the other samples were determined relative to this sample ("normalized"). Phosphoprotein levels were then corrected to account for the normalized loading control level for each sample (ie. γH2AX level divided by normalized GAPDH).

Biochemical Fractionation

Fractionation experiments were carried out as previously described[28]. Treated or mock treated cells were washed with ice-cold PBS and cell fractionation was carried out by consecutive extractions with increasing detergent concentration. Cell pellets were first resuspended for 5 min on ice in fractionation buffer I (50mM HEPES, pH 7.5; 150mM NaCl; 1mM EDTA; 0.2% IGEPAL CA-630), supplemented with protease and phosphatase inhibitors. Following centrifugation at 1000 × g for 5 min, the supernatant was collected (fraction I, cytoplasmic), and the pellets were washed with the same buffer. The nuclear pellets were further extracted for 40 min on ice with fractionation buffer II (50mM HEPES, pH 7.5; 150mM NaCl; 1mM EDTA; 0.5% IGEPAL CA-630). The extracts were clarified by centrifugation at 16,000 × g for 15 min (supernatant is fraction II, nuclear). The pellets were finally lysed in RIPA buffer (150mM NaCl; 1% NP-40; 0.5% $C_{24}H_{39}O_4Na$; 0.1% SDS; 50mM Tris-HCl, pH 8.0), sonicated, and cleared by centrifugation at 16,000 × g for 20 min (fraction III, chromatin). Equal aliquots of each fraction, determined by BCA assay, were separated and immunoblotted as above.

Immunofluorescence

For γH2AX and 53BP1 immunofluorescence, MEFs were grown on glass coverslips in 6-well plates, treated with 10 Gy of IR (^{137}Cs) with a 30 min incubation post-IR. MEFs were fixed in 3% paraformaldehyde/2% sucrose at RT and permeabilized with TX100 solution (0.5% TritonX-100; 20mM HEPES, pH7.4; 50nM NaCl; 3mM $MgCl_2$; 300mM sucrose) on ice. Cells were incubated with monoclonal mouse γH2AX antibody (1:1000, EMD Millipore, #05-636) or 53BP1 (1:200, Novus Biologicals, #NB100-904) in PBS with 5% goat serum for 20 min at 37°C. Validation these primary antibodies was provided by the manufacturer. Cells were then incubated with goat anti-mouse AlexaFluor 488 antibody (1:800, Molecular Probes, #A11001) or goat anti-rabbit AlexaFluor 594 (1:800, Molecular Probes, #A11012) antibody in PBS/5% goat serum for 20 min at 37°C. Coverslips were then fixed on slides using ProLong® Gold Antifade Reagent with DAPI (Life Technologies). The investigator was blinded for the scoring of foci.

IR Sensitivity Assays

MEFs were plated in a 12-well dish at a low density (500-8000 cells/well) and allowed to attach overnight. Cells were then treated with varying doses of IR and allowed to grow until the unirradiated control well for each genotype reached confluency (5 to 7 days). Cellular survival was determined using a crystal violet colorimetric assay, as previously described[57].

Laser Microirradiation and Live Cell Imaging

MEFs were transfected with MDC1-BRCT-eGFP, Ku70-GFP, Ku80-GFP, or GFP-NBS1 on glass-bottomed culture dishes (MatTek Corporation). Laser microirradiation was performed as previously published[58]. Damage was induced using an IX 71 microscope (Olympus) coupled with the MicroPoint Laser Illumination and Ablation System (Photonic Instruments). A 337.1 nm laser diode (3.4 mW) transmits through a specific dye cell and then yields a 365 nm wavelength laser beam that is focused through a 603 UPlanSApo/1.35 oil objective to yield a spot size of 0.5–1 mm. The pulse energy is 170 mJ at 10 Hz and the time of cell exposure to the laser beam was around 3.5 ns. Images were taken using the same microscope with the CellSense software (Olympus). Analysis of GFP fluorescence at the site of damage was converted into a numerical value (fluorescence intensity) using ImageJ software.

G2/M Checkpoint Assays

5×10^5 MEFs were plated per 10 cm dish, grown for 48 hr, treated with or without 10 Gy IR (^{137}Cs), allowed to recover for 1 hr and fixed. Cells were analyzed for the mitotic marker phospho-histone $H3^{S10}$ (Cell Signaling, #9706)[59] and FITC-conjugated secondary antibody (BD Biosciences, #553443). Flow cytometry was carried out on an Accuri C6 Flow Cytometer (BD Biosciences) as previously described[60]. Data was analyzed using FlowJo.

Recombination Assays

The DR-GFP reporter has been described previously[26]. The plasmid was integrated into the genome of MEFs via transfection with X-tremeGENE 9 (Roche) and colonies were selected in puromycin (2.5μg/ml). Single copy intact integration was confirmed by Southern blot. I-SceI was transiently expressed via infection with *I-SceI* containing adenovirus (AdNGUS24i), and recombination frequency determined as the % GFP^+ cells 3 days post-infection. Background levels of GFP were determined by infecting cells with an empty adenovirus for comparison. Flow cytometry was carried out on an Accuri C6 Flow Cytometer (BD Biosciences). Data was analyzed using FlowJo.

Supplementary Material

Refer to Web version on PubMed Central for supplementary material.

Acknowledgments

The authors thank X. Yu (University of Michigan) for reagents and for use of the laser microirradiation apparatus, M. Jasin (Memorial Sloan Kettering Cancer Center) for the DR-GFP reporter, F. Graham and P. Ng (McMaster University) for the AdNGUS24i *I-SceI* adenovirus, and J. Sekiguchi for helpful discussions regarding the manuscript. Support for this work was provided by the US National Institutes of Health R01-HL079118 (DOF), a

Leukemia and Lymphoma Society Scholar Grant (DOF) and the University of Michigan Cancer Center Support Grant 5-P30-CA46592. AJH was supported by T32 CA009676 and MJM by T32 AI007413.

References

1. Jackson SP, Bartek J. The DNA-damage response in human biology and disease. Nature. 2009; 461:1071–8. [PubMed: 19847258]
2. Symington LS, Gautier J. Double-Strand Break End Resection and Repair Pathway Choice. Annu Rev Genet. 2010
3. Ciccia A, Elledge SJ. The DNA damage response: making it safe to play with knives. Mol Cell. 2010; 40:179–204. [PubMed: 20965415]
4. Goodarzi AA, Jeggo PA. The repair and signaling responses to DNA double-strand breaks. Adv Genet. 2013; 82:1–45. [PubMed: 23721719]
5. Falck J, Coates J, Jackson SP. Conserved modes of recruitment of ATM, ATR and DNA-PKcs to sites of DNA damage. Nature. 2005; 434:605–11. [PubMed: 15758953]
6. Matsuoka S, et al. ATM and ATR substrate analysis reveals extensive protein networks responsive to DNA damage. Science. 2007; 316:1160–6. [PubMed: 17525332]
7. McKinnon PJ. ATM and the molecular pathogenesis of ataxia telangiectasia. Annu Rev Pathol. 2012; 7:303–21. [PubMed: 22035194]
8. Uziel T, et al. Requirement of the MRN complex for ATM activation by DNA damage. EMBO J. 2003; 22:5612–21. [PubMed: 14532133]
9. Lee JH, Paull TT. Activation and regulation of ATM kinase activity in response to DNA double-strand breaks. Oncogene. 2007; 26:7741–8. [PubMed: 18066086]
10. Shiloh Y, Ziv Y. The ATM protein kinase: regulating the cellular response to genotoxic stress, and more. Nat Rev Mol Cell Biol. 2013; 14:197–210.
11. Price BD, D'Andrea AD. Chromatin remodeling at DNA double-strand breaks. Cell. 2013; 152:1344–54. [PubMed: 23498941]
12. Lee JH, Paull TT. ATM activation by DNA double-strand breaks through the Mre11-Rad50-Nbs1 complex. Science. 2005; 308:551–4. [PubMed: 15790808]
13. Stracker TH, Roig I, Knobel PA, Marjanovic M. The ATM signaling network in development and disease. Front Genet. 2013; 4:37. [PubMed: 23532176]
14. Buis J, et al. Mre11 nuclease activity has essential roles in DNA repair and genomic stability distinct from ATM activation. Cell. 2008; 135:85–96. [PubMed: 18854157]
15. Dupre A, Boyer-Chatenet L, Gautier J. Two-step activation of ATM by DNA and the Mre11-Rad50-Nbs1 complex. Nat Struct Mol Biol. 2006; 13:451–7. [PubMed: 16622404]
16. Dynan WS, Yoo S. Interaction of Ku protein and DNA-dependent protein kinase catalytic subunit with nucleic acids. Nucleic Acids Res. 1998; 26:1551–9. [PubMed: 9512523]
17. Walker JR, Corpina RA, Goldberg J. Structure of the Ku heterodimer bound to DNA and its implications for double-strand break repair. Nature. 2001; 412:607–14. [PubMed: 11493912]
18. Davis AJ, Chen BP, Chen DJ. DNA-PK: a dynamic enzyme in a versatile DSB repair pathway. DNA Repair (Amst). 2014; 17:21–9. [PubMed: 24680878]
19. Gao Y, et al. A targeted DNA-PKcs-null mutation reveals DNA-PK-independent functions for KU in V(D)J recombination. Immunity. 1998; 9:367–76. [PubMed: 9768756]
20. Jhappan C, Morse HC 3rd, Fleischmann RD, Gottesman MM, Merlino MM. DNA-PKcs:a T-cell tumour suppressor encoded at the mouse scid locus. Nat Genet. 1997; 17:483–6. [PubMed: 9398856]
21. Gu Y, et al. Growth retardation and leaky SCID phenotype of Ku70-deficient mice. Immunity. 1997; 7:653–65. [PubMed: 9390689]
22. Carson CT, et al. The Mre11 complex is required for ATM activation and the G2/M checkpoint. EMBO J. 2003; 22:6610–20. [PubMed: 14657032]
23. Shiloh Y. ATM and related protein kinases: safeguarding genome integrity. Nat Rev Cancer. 2003; 3:155–68. [PubMed: 12612651]

24. Bressan DA, Baxter BK, Petrini JH. The Mre11-Rad50-Xrs2 protein complex facilitates homologous recombination-based double-strand break repair in Saccharomyces cerevisiae. Mol Cell Biol. 1999; 19:7681–7. [PubMed: 10523656]
25. Tomita K, et al. Competition between the Rad50 complex and the Ku heterodimer reveals a role for Exo1 in processing double-strand breaks but not telomeres. Mol Cell Biol. 2003; 23:5186–97. [PubMed: 12861005]
26. Pierce AJ, Johnson RD, Thompson LH, Jasin M. XRCC3 promotes homology-directed repair of DNA damage in mammalian cells. Genes Dev. 1999; 13:2633–8. [PubMed: 10541549]
27. Helleday T. Pathways for mitotic homologous recombination in mammalian cells. Mutat Res. 2003; 532:103–15. [PubMed: 14643432]
28. Andegeko Y, et al. Nuclear retention of ATM at sites of DNA double strand breaks. J Biol Chem. 2001; 276:38224–30. [PubMed: 11454856]
29. Rogakou EP, Boon C, Redon C, Bonner WM. Megabase chromatin domains involved in DNA double-strand breaks in vivo. J Cell Biol. 1999; 146:905–16. [PubMed: 10477747]
30. Xu X, Stern DF. NFBD1/KIAA0170 is a chromatin-associated protein involved in DNA damage signaling pathways. J Biol Chem. 2003; 278:8795–803. [PubMed: 12499369]
31. Stucki M, et al. MDC1 directly binds phosphorylated histone H2AX to regulate cellular responses to DNA double-strand breaks. Cell. 2005; 123:1213–26. [PubMed: 16377563]
32. Lou Z, et al. MDC1 maintains genomic stability by participating in the amplification of ATM-dependent DNA damage signals. Mol Cell. 2006; 21:187–200. [PubMed: 16427009]
33. Fernandez-Capetillo O, et al. DNA damage-induced G2-M checkpoint activation by histone H2AX and 53BP1. Nat Cell Biol. 2002; 4:993–7. [PubMed: 12447390]
34. Lan L, et al. Accumulation of Werner protein at DNA double-strand breaks in human cells. J Cell Sci. 2005; 118:4153–62. [PubMed: 16141234]
35. Shibata A, et al. DNA double-strand break repair pathway choice is directed by distinct MRE11 nuclease activities. Mol Cell. 2014; 53:7–18. [PubMed: 24316220]
36. Williams RS, et al. Mre11 dimers coordinate DNA end bridging and nuclease processing in double-strand-break repair. Cell. 2008; 135:97–109. [PubMed: 18854158]
37. Zou L, Elledge SJ. Sensing DNA damage through ATRIP recognition of RPA-ssDNA complexes. Science. 2003; 300:1542–8. [PubMed: 12791985]
38. Stiff T, et al. ATR-dependent phosphorylation and activation of ATM in response to UV treatment or replication fork stalling. EMBO J. 2006; 25:5775–82. [PubMed: 17124492]
39. Prevo R, et al. The novel ATR inhibitor VE-821 increases sensitivity of pancreatic cancer cells to radiation and chemotherapy. Cancer Biol Ther. 2012; 13:1072–81. [PubMed: 22825331]
40. Bakkenist CJ, Kastan MB. DNA damage activates ATM through intermolecular autophosphorylation and dimer dissociation. Nature. 2003; 421:499–506. [PubMed: 12556884]
41. Pellegrini M, et al. Autophosphorylation at serine 1987 is dispensable for murine Atm activation in vivo. Nature. 2006; 443:222–5. [PubMed: 16906133]
42. Sun J, Lee KJ, Davis AJ, Chen DJ. Human Ku70/80 protein blocks exonuclease 1-mediated DNA resection in the presence of human Mre11 or Mre11/Rad50 protein complex. J Biol Chem. 2012; 287:4936–45. [PubMed: 22179609]
43. Langerak P, Mejia-Ramirez E, Limbo O, Russell P. Release of Ku and MRN from DNA Ends by Mre11 Nuclease Activity and Ctp1 Is Required for Homologous Recombination Repair of Double-Strand Breaks. PLoS Genet. 2011; 7:e1002271. [PubMed: 21931565]
44. Shao Z, et al. Persistently bound Ku at DNA ends attenuates DNA end resection and homologous recombination. DNA Repair (Amst). 2012; 11:310–6. [PubMed: 22265216]
45. Blier PR, Griffith AJ, Craft J, Hardin JA. Binding of Ku protein to DNA. Measurement of affinity for ends and demonstration of binding to nicks. J Biol Chem. 1993; 268:7594–601. [PubMed: 8463290]
46. Paull TT, Deshpande RA. The Mre11/Rad50/Nbs1 complex: Recent insights into catalytic activities and ATP-driven conformational changes. Exp Cell Res. 2014
47. Deshpande RA, et al. ATP-driven Rad50 conformations regulate DNA tethering, end resection, and ATM checkpoint signaling. EMBO J. 2014; 33:482–500. [PubMed: 24493214]

48. Difilippantonio S, et al. Distinct domains in Nbs1 regulate irradiation-induced checkpoints and apoptosis. J Exp Med. 2007; 204:1003–11. [PubMed: 17485521]
49. Stracker TH, Morales M, Couto SS, Hussein H, Petrini JH. The carboxy terminus of NBS1 is required for induction of apoptosis by the MRE11 complex. Nature. 2007; 447:218–21. [PubMed: 17429352]
50. Smith GC, et al. Purification and DNA binding properties of the ataxia-telangiectasia gene product ATM. Proc Natl Acad Sci U S A. 1999; 96:11134–9. [PubMed: 10500142]
51. Hickson I, et al. Identification and characterization of a novel and specific inhibitor of the ataxia-telangiectasia mutated kinase ATM. Cancer Res. 2004; 64:9152–9. [PubMed: 15604286]
52. Nakada S, et al. Non-canonical inhibition of DNA damage-dependent ubiquitination by OTUB1. Nature. 2010; 466:941–6. [PubMed: 20725033]
53. Nutley BP, et al. Preclinical pharmacokinetics and metabolism of a novel prototype DNA-PK inhibitor NU7026. Br J Cancer. 2005; 93:1011–8. [PubMed: 16249792]
54. Zha S, et al. Ataxia telangiectasia-mutated protein and DNA-dependent protein kinase have complementary V(D)J recombination functions. Proc Natl Acad Sci U S A. 2011; 108:2028–33. [PubMed: 21245310]
55. Regal JA, Festerling TA, Buis JM, Ferguson DO. Disease-associated MRE11 mutants impact ATM/ATR DNA damage signaling by distinct mechanisms. Hum Mol Genet. 2013
56. Wang RH, et al. Impaired DNA damage response, genome instability, and tumorigenesis in SIRT1 mutant mice. Cancer Cell. 2008; 14:312–23. [PubMed: 18835033]
57. Taniguchi T, et al. Convergence of the fanconi anemia and ataxia telangiectasia signaling pathways. Cell. 2002; 109:459–72. [PubMed: 12086603]
58. Li M, Yu X. Function of BRCA1 in the DNA damage response is mediated by ADP-ribosylation. Cancer Cell. 2013; 23:693–704. [PubMed: 23680151]
59. Van Hooser A, Goodrich DW, Allis CD, Brinkley BR, Mancini MA. Histone H3 phosphorylation is required for the initiation, but not maintenance, of mammalian chromosome condensation. J Cell Sci. 1998; 111(Pt 23):3497–506. [PubMed: 9811564]
60. Theunissen JW, Petrini JH. Methods for studying the cellular response to DNA damage: influence of the Mre11 complex on chromosome metabolism. Methods Enzymol. 2006; 409:251–84. [PubMed: 16793406]

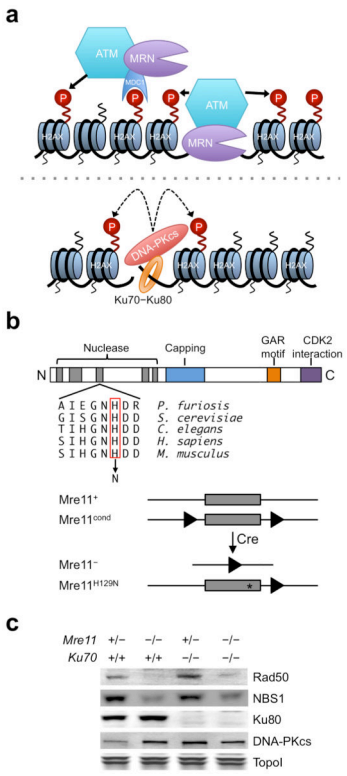

Figure 1. The early response to DNA DSBs

a, Prevailing model of DSB sensing and the initiation of kinase signaling. **b**, Mammalian Mre11 domain structure (top) and engineered murine germline *Mre11* alleles (bottom)[14]. Red rectangle, histidine in exon 5 (grey box) essential for nuclease activities; line, introns; triangles, LoxP sites; asterisk, H129N mutation. **c,** Immunoblot of Rad50, NBS1, Ku80, and DNA-PKcs levels in cells of indicated genotypes. TopoI is the protein loading control.

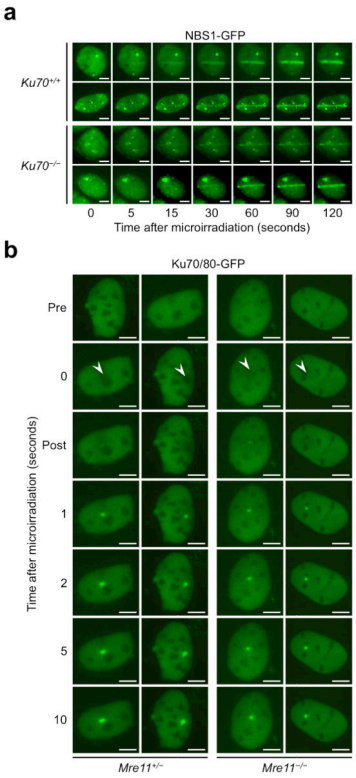

Figure 2. MRN and Ku relocate to DSBs independently in the early DSB response

a and b, Live cell imaging of MRN **(a)** and Ku **(b)** relocation to laser microirradiation-induced damage. Panels show two representative cells per genotype. n=3 cell culture replicates. Scale bars shown are 10 μm. **a**, GFP-tagged NBS1 was monitored in live cells by time-lapse photography during fluorescent microscopy. **b**, GFP-tagged Ku70/80 was monitored in live cells via fluorescent microscopy video capture. Individual frames corresponding to indicated time points (left) are shown. Arrow; spot of laser target.

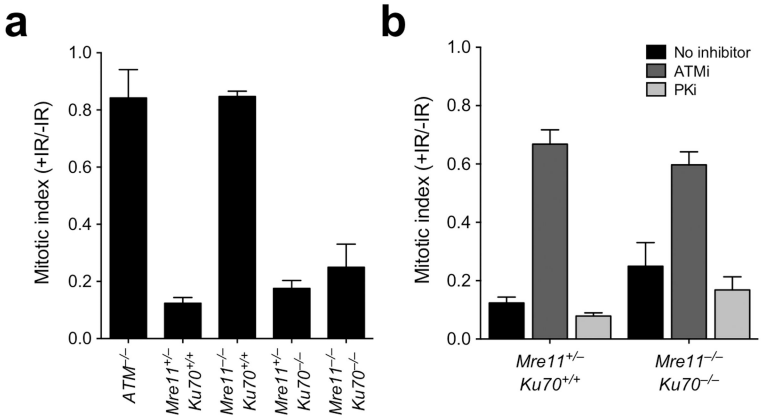

Figure 3. Ku loss bypasses the need for MRN in activating the G2/M checkpoint

a, Assessment of the G2/M checkpoint by comparing mitotic indices (% phospho-histone $H3^{S10}$ positive cells) before and 1 hour after 10 Gy IR. Mitotic index; +IR to –IR ratio. Shorter bars reflect intact checkpoint function. Bars represent the mean and error bars the s.e.m. (n=3 cell culture replicates). **b,** Assessment of the G2/M checkpoint in cells pretreated ± kinase inhibitors (ATM inhibitor, ATMi; DNA-PK inhibitor, PKi) as in (a).

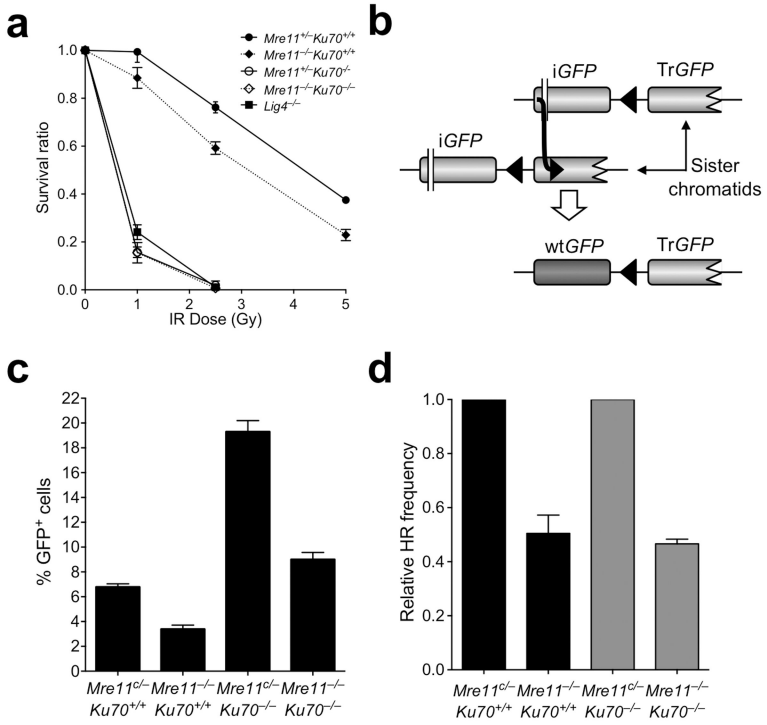

Figure 4. Ku loss does not bypass the need for MRN in DSB repair

a, IR sensitivities expressed as the survival ratio relative to unirradiated control. Bars represent the mean and error bars the s.e.m. (n=3 cell culture replicates). **b,** Schematic of assay to measure HDR of a site-specific DSB (DR-GFP)[26]. **c,** The absolute frequencies of HDR. Bars represent the mean and error bars the s.e.m. (n=3 cell culture replicates). **d,** The relative frequencies of HDR. To determine the relative frequency of HDR, percentages were normalized to *Mre11*$^{c/-}$ control lines, which were set to 1.0. Bars represent the mean and error bars the s.e.m. (n=3 cell culture replicates).

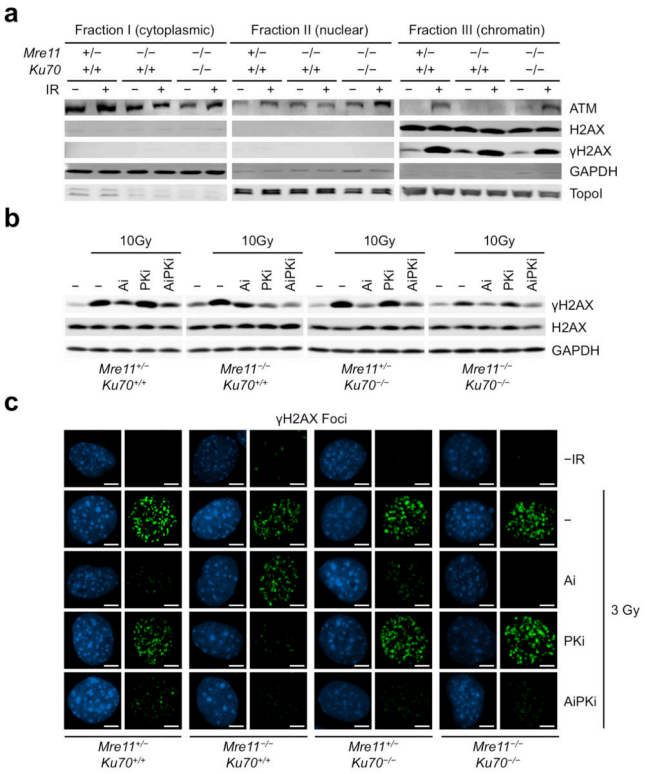

Figure 5. ATM recruitment and activation in the absence of DSB sensors

a, Immunoblot of protein levels in cellular fractions (top) prepared 30 min after ± IR. Genotypes are also listed at the top. **b,** Immunoblot of γH2AX levels 30 minutes post-IR after pretreatment ± kinase inhibitors (ATM inhibitor, ATMi; DNA-PK inhibitor, PKi; ATM and DNA-PK inhibitors, AiPKi). GAPDH is the protein loading control. Genotypes are at the bottom. For uncropped images from **a** and **b**, see Supplemental Data Set 1. **c,** γH2AX immunofluorescent foci (green) 30 min post-IR ± kinase inhibitors (Ai, PKi, AiPKi). Nuclei are stained with DAPI (blue). Genotypes are at the bottom. Scale bars shown are 10 μm.

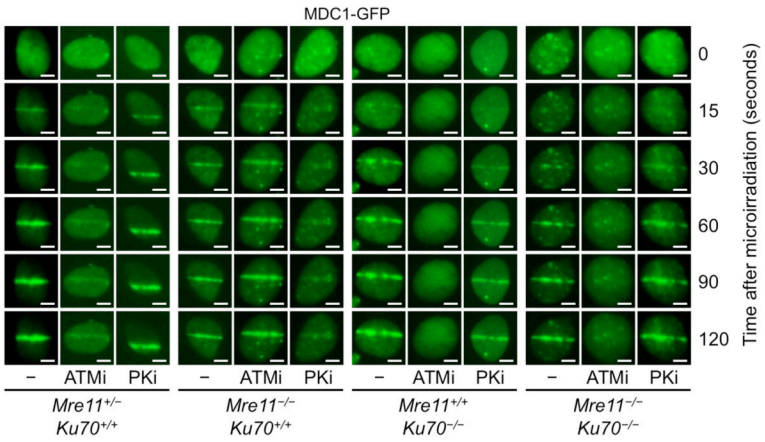

Figure 6. MDC1 recruitment in the absence of MRN and Ku

Recruitment kinetics of the MDC1 protein. The BRCT domain of MDC1 was tagged with GFP and expressed in cells of the indicated genotypes (bottom). Live cells pretreated ± kinase inhibitors (ATM inhibitor, ATMi; DNA-PK inhibitor, PKi) were exposed to laser microirradiation and monitored by time-lapse photography at the indicated times (right). Panels show one representative cell per genotype and condition. n=3 cell culture replicates. Scale bars shown are 10 μm.

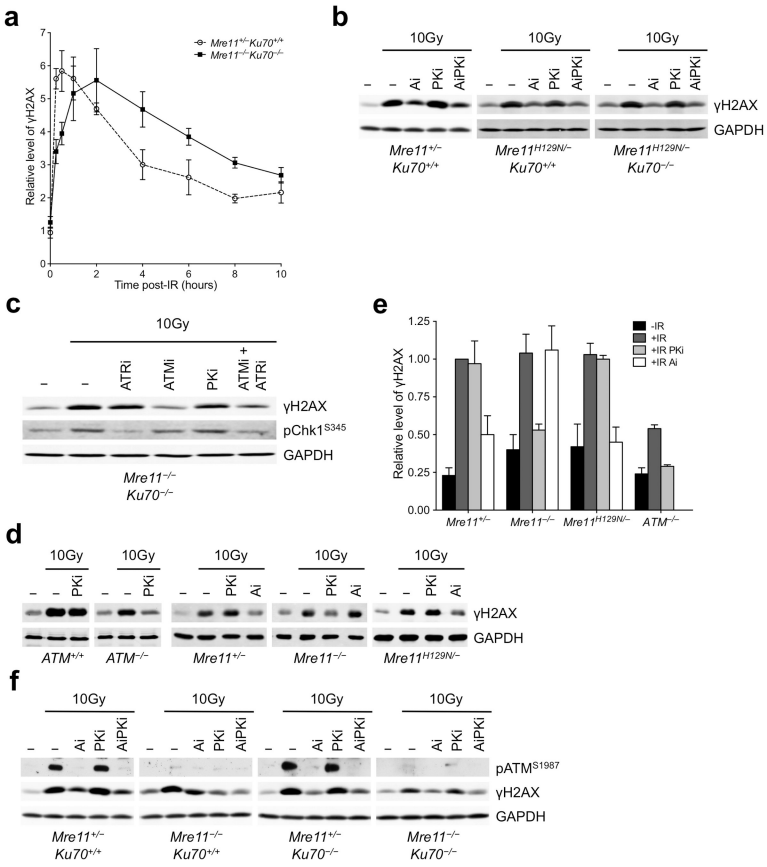

Figure 7. Comparisons of ATM activation in the presence versus absence of DSB sensors

a, Timecourse of relative γH2AX levels quantified from immunoblots (an example is shown in Figure S5d). Bars represent the mean and error bars the s.e.m. (n=3 cell culture replicates). **b,** Immunoblot comparing γH2AX levels ±10 Gy of IR after pretreatment with (ATM inhibitor, ATMi; DNA-PK inhibitor, PKi; ATM and DNA-PK inhibitors, AiPKi) or without (–) kinase inhibitor 30 minutes post-IR to determine the impact of Mre11 nuclease deficiency (*Mre11*^{H129N}). **c,** Immunoblot of γH2AX and phosphorylated Chk1 levels ±10 Gy of IR after pretreatment with (ATR inhibitor, ATRi; ATMi; PKi) or without (–) kinase inhibitor 30 minutes post-IR. **d,** Comparison of γH2AX levels in sensor versus kinase deficiencies. **e,** Quantitation of γH2AX levels from immunoblot in (d) and two additional experiments. Bars represent the mean and error bars the s.e.m. (n=3 cell culture replicates). **f,** Immunoblot as in Figure 5b comparing pATM^{S1987} levels from these same extracts (for uncropped images see Supplementary Data Set 1).